Journal of Structural Geology, Vol. 13, No. 8, pp. 927 to 943, 1991
Printed in Great Britain

0191-8141/91 $03.00+0.00

Change in dominant mechanisms for phyllosilicate preferred orientation during cleavage development in the Kitakami slates of NE Japan

KYUICHI KANAGAWA*

Department of Geology and Geography, University of Massachusetts, Amherst, MA 01003, U.S.A.

(*Received* 18 *June* 1990; *accepted in revised form* 20 *February* 1991)

Abstract—Selected slates from the Kitakami Mountains of NE Japan were studied by means of finite strain measurement, X-ray texture goniometry, optical microscopy, back-scattered SEM, and X-ray fluorescence and diffraction analyses.

Finite strain recorded by radiolarians in slates, although not equivalent to bulk strain, shows a positive correlation with strength of phyllosilicate basal plane fabrics. However, there is a possible difference between the fabric pattern and radiolarian strain ellipsoid shape as well as a difference in fabric pattern between chlorite and illite/mica. These relationships between phyllosilicate fabrics and finite strains suggest that strain estimation from phyllosilicate fabrics based on the March model may be unreliable unless their relationship is established in each case.

Optical and back-scattered SEM studies revealed a change in microstructures in accordance with increasing fabric strength. In slates with weak fabric strength, cleavage domains are dark to opaque in appearance and characterized by a concentration of insoluble residues such as carbonaceous matter, sphene, ilmenite, rutile, epidote and apatite as well as phyllosilicates. Phyllosilicates in cleavage domains are oriented subparallel to cleavage, whereas those in intercleavage domains are variously oriented. As fabric strength increases, cleavage domains become transparent and composed mainly of phyllosilicates. Phyllosilicates become finer-grained and more uniform in grain size. They are well oriented in both cleavage and intercleavage domains. As fabric strength further increases, phyllosilicates tend to coarsen.

These lines of microstructural evidence suggest that the dominant mechanism for phyllosilicate preferred orientation changes as cleavage develops from pressure solution transfer, through syntectonic crystallization–recrystallization, and possibly to oriented grain growth. Because fabric strength increases with increasing illite crystallinity, metamorphic grade (mainly temperature) must be one of the major factors which control the dominance of phyllosilicate preferred orientation mechanisms.

INTRODUCTION

SLATY cleavage is the most distinctive planar fabric found in low-grade metamorphic rocks and has been studied by a number of structural geologists. Studies during the past two centuries revealed three principal mechanisms for phyllosilicate preferred orientation leading to slaty cleavage development: (1) mechanical rotation due to strain; (2) syntectonic crystallization and/or recrystallization in association with oriented grain growth; and (3) passive reorientation as matrix minerals are removed by pressure solution transfer (e.g. Siddans 1972, Wood 1974, White & Knipe 1978, Borradaile *et al.* 1982).

If initially randomly oriented phyllosilicates rotate mechanically due to homogeneous strain as in the model proposed by March (1932), the resulting preferred orientation would be directly related to finite strain. In fact, several examples of preferred orientation of phyllosilicates obtained from naturally and experimentally deformed specimens seem to be consistent with those estimated from the March model (Means & Paterson 1966, Tullis & Wood 1975, Tullis 1976, Wood *et al.* 1976, Wood & Oertel 1980). Other examples are, however, inconsistent with the model (Clark 1970, Holeywell & Tullis 1975, Siddans 1976, 1977, Etheridge & Oertel 1979, Gapais & Brun 1981). The March model has been so attractive to some workers (e.g. Oertel 1983, 1985) that they still estimate strains from phyllosilicate fabrics based on this model without any consideration of microstructural features (e.g. Chen & Oertel 1989, Oertel *et al.* 1989).

In contrast, many studies based upon microstructural observations and microchemical analyses have revealed the importance of pressure solution transfer and syntectonic crystallization–recrystallization together with metamorphic reactions in slaty cleavage development (e.g. Durney 1972, Williams 1972, Etheridge *et al.* 1974, Etheridge & Lee 1975, Holeywell & Tullis 1975, Means 1975, Gray 1977, 1978, 1979, Knipe & White 1977, White & Knipe 1978, Knipe 1979, 1981, Stephens *et al.* 1979, White & Johnston 1981, Borradaile *et al.* 1982, Woodland 1982, Lee *et al.* 1986, Sutton 1989).

The above three mechanisms may compete with each other during cleavage development in slates, and their relative importance may change as cleavage develops or as geological conditions vary (Ramsay & Huber 1983, p. 185). In some slates, mechanical rotation associated with microcrenulation may have been followed by syntectonic crystallization–recrystallization (Tullis 1976, Roy 1978, White & Knipe 1978, Knipe 1981, White & Johnston 1981). In other slates microcrenulation may have been followed by pressure solution transfer (Williams 1972, Cosgrove 1976, Gray 1977, 1978, 1979) and later by syntectonic crystallization (Weber 1981). In still

* Present address: Department of Geology, University of Tokyo, Tokyo 113, Japan.

other slates mechanical rotation may have never been significant during cleavage development (Etheridge & Lee 1975, Holeywell & Tullis 1975, Woodland 1982, Gregg 1985, Lee *et al.* 1986, Ishii 1988a). However, the controls on their relative importance and the transition between the three mechanisms are still not well understood.

In order to evaluate the mechanisms for phyllosilicate preferred orientation, selected slates from the Kitakami Mountains of NE Japan (Fig. 1) were studied by means of finite strain measurement, X-ray texture goniometry, optical microscopy, back-scattered SEM, and X-ray fluorescence and diffraction analyses. The results are not consistent with the March model, and suggest a change in dominant mechanisms for phyllosilicate preferred orientation during cleavage development.

GEOLOGICAL SETTING

The Kitakami Mountains are the best-known slate belt in Japan. They are divided into two structurally NNW-trending sectors, southwestern and northeastern, which represent a pre-Cretaceous island arc and a fore-arc, respectively. Silurian to earliest Cretaceous shallow marine sedimentary and volcanic rocks were deposited on pre-Silurian granite and pre-Devonian (probably Ordovician) ophiolite basements in the southwestern Kitakami Mountains, whereas Permian to Jurassic accretionary sediments are mainly distributed in the northeastern Kitakami Mountains (Kato 1985, Ehiro *et al.* 1988, Ozawa *et al.* 1988). Early Cretaceous volcanic and sedimentary rocks and granitic plutons are distributed across the older NNW structural trend over the Kitakami Mountains.

Strata in the Kitakami Mountains were folded and cleaved during Early Cretaceous deformation and metamorphism. Macroscopic folds trending N to NNW initiated as flexural-slip folds, and were subsequently flattened during the formation of slaty cleavage trending N to NNE and dipping steeply (Kanagawa 1986). Transected folds accompanied by non-axial plane cleavage are consequently recognized in some places (Takizawa 1981, Ishii 1985, Kanagawa 1986). The regional metamorphism under which slaty cleavage was formed is considered to be closely related to a rise in temperature caused by granite plutonism (Oho 1982, Ikeda 1984, Kanagawa 1985, Ishii 1988b). The emplacement of granite plutons, however, may have been slightly after the peak of regional deformation and metamorphism as indicated by growth of biotite porphyroblasts over cleavage textures (Ishii 1988b), and locally caused ductile aureole deformation (Kanagawa 1985).

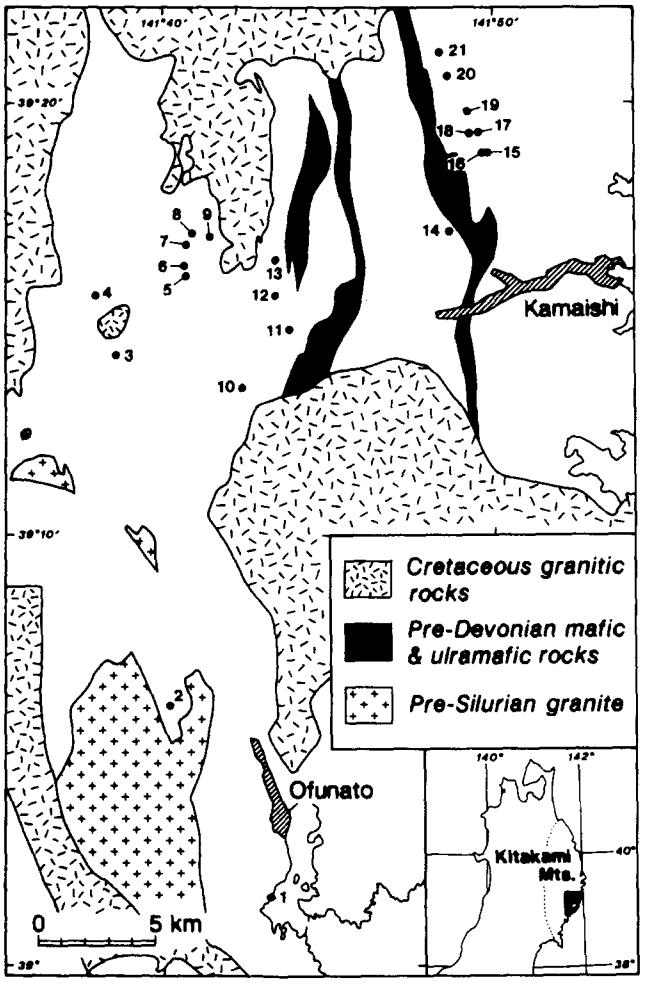

Fig. 1. Locality map of studied slate samples in the central-eastern part of the Kitakami Mountains. Sample at locality 2 is Devonian, samples at 10 and 12 are Carboniferous, and other samples are Permian in age.

EXPERIMENTAL PROCEDURES

Sample selection

From more than 500 slate samples collected in a central-eastern part of the Kitakami Mountains, 21 samples (one Devonian, two Carboniferous, 18 Permian) were selected (Fig. 1) for the following reasons. (1) They include abundant radiolarians most of which were initially spherical so that finite strains recorded by them can be determined. (2) They are fine-grained rather homogeneous black argillaceous slates, presumably with little variation in initial grain size and chemistry. (3) They have been affected to varying degrees by thermal metamorphism due to granite plutons, and the effect of metamorphic temperature on cleavage development is expected to be significant (Oho 1982, Ishii 1988a,b). (4) They are all in chlorite zones but outside biotite zones of contact aureoles, and their cleavage textures are not disturbed by contact metamorphism (Ishii 1988b). (5) They possess slaty cleavage developed to various degrees so that deformational processes in slates may be examined. However, these samples were not systematically collected in the way which allows the analysis of progressive deformation in slates.

Because not all the samples collected were oriented, and because it was difficult in many slate samples to determine stretching or mineral lineation, specimen coordinates were chosen in this paper such that the x axis is

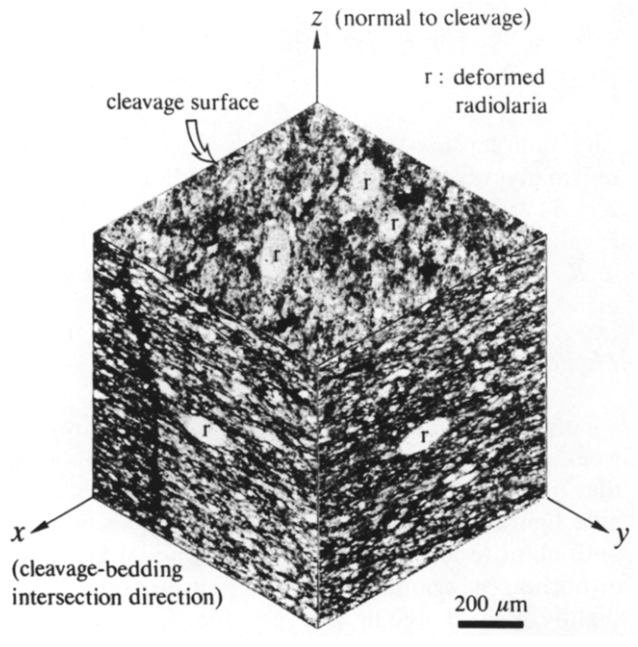

Fig. 2. Specimen co-ordinates with reference to cleavage and bedding, used in this study.

parallel to the cleavage–bedding intersection lineation and the z axis normal to cleavage surface (Fig. 2). In slates with cleavage almost parallel to bedding, x axes were arbitrarily chosen in the cleavage surface. However, it should be noted that the attitudes of cleavage–bedding intersections vary considerably in the sampling area due to the non-axial planar nature of cleavage (Kanagawa 1986).

Strain analysis of radiolarians

In order to determine the finite strain recorded by radiolarians, three orthogonal thin sections, the xy section parallel to cleavage surface, yz section normal to cleavage–bedding intersection and xz section normal to the other two sections, were prepared from each sample (Fig. 2). Radiolarians were then traced either from photomicrographs or universal projections. Axial lengths and long-axis orientations of 60–330 (average about 150) radiolarians were obtained from each of these three sections using an image analysis system which allows rapid and precise data collection (details in Kanagawa 1990). After applying R_f/ϕ symmetry tests according to Dunnet & Siddans (1971), averaged final shape matrices (Shimamoto & Ikeda 1976), $\bar{S}_{xy}$, $\bar{S}_{yz}$ and $\bar{S}_{xz}$, were calculated. The strain ellipsoid matrix (λ'_{ij}) was then determined from these three matrices using the method described in Shimamoto & Ikeda (1976), and diagonalized to obtain principal strain axes (X, Y and Z) and principal-plane strain ratios (R_{XY}, R_{YZ} and R_{XZ}).

The existence of pressure shadows around radiolarians as well as the material difference between matrix and radiolarian skeleton dominantly occupied by quartz (Fig. 2) indicate that finite strains recorded by radiolarians, designated radiolarian strains hereafter, must be smaller than bulk finite strains. However, it may be reasonable to assume that there is a correlation between radiolarian strain and bulk strain.

X-ray texture goniometry

For each slate sample, preferred orientations of chlorite (002) and illite–mica (004) were measured using an automated Rigaku X-ray texture goniometer with Cu Kα radiation at 40 kV and 30 mA (details in Kanagawa & Yoshida 1988). Uniformly thin disks cut parallel to cleavage with diameters ranging from 20 to 30 mm and μt values (μ, linear absorption coefficient; t, specimen thickness) ranging from 0.3 to 1.2 were prepared for measurement. The specimens were vacuum-impregnated with epoxy prior to grinding so that the phyllosilicate grains were not significantly affected by preparation procedures (see Kanagawa & Yoshida 1988 for preparation). Complete pole figures were obtained from combined transmission and reflection mode step scans (Siddans 1976, Wenk 1985) with 5° tilt intervals and 10° azimuth intervals. Phyllosilicate preferred orientation measurement of cleavage-parallel sections using this method is acceptable as long as relative variations of preferred orientation are examined (see Appendix). The reflection scan covers the central part of a pole figure with polar angles of 0–60°, while the transmission scan covers the peripheral part with polar angles of 60–90°. The counting time at each tilt–azimuth position for peak and two background 2θ angles was 10 s for chlorite (002) and 30 s for illite/mica (004) because of its weak intensity. A complete measurement took 8 h for chlorite and 24 h for illite/mica.

Optical and back-scattered electron microscopy

Five slate samples were chosen for detailed microstructural observations. Extremely thin (less than 10 μm) polished thin sections normal to both cleavage and bedding (yz sections) were prepared from the five samples. These were vacuum-impregnated with epoxy twice prior to thin-sectioning and polishing, respectively, in order to prevent damage during preparation procedures.

After observations under the optical microscope with transmitted and reflected light, back-scattered electron (BSE) images were observed using a JEOL scanning electron microscope with a LINK energy dispersive analysis system at working distances of 15 and 37 mm, accelerating voltage of 15 kV, and beam current of 10^{-9} A. BSE images provide useful information on the microstructure of fine-grained sediments (e.g. Krinsley *et al.* 1983, White *et al.* 1984, Agar *et al.* 1989).

Grain size distribution of phyllosilicates

Grains (170–700) excluding large detrital grains, were traced for chlorite and illite and/or muscovite from BSE micrographs of each of the above five samples. The area of each grain was obtained through image analysis (cf. Kanagawa 1990), and its grain size was calculated as the

diameter of a circle with the same area. Grain size distributions of chlorite and illite/muscovite in each sample were then represented as normalized histograms of every 0.2 μm size fractions.

Whole-rock chemistry

The remaining samples were crushed and prepared for X-ray fluorescence, carbon and X-ray diffraction analyses. Major elements were analyzed using a Rigaku X-ray fluorescence spectroscopy together with a LECO carbon determinator. Total carbon content of organic carbon and carbonate carbon (C in CO_2 or CO_3) is obtained and represented in weight % by using the carbon determinator.

Illite crystallinity

The ratio of illite/mica peak height at 10 Å to that at 10.5 Å (sharpness ratio or Weaver Index) was measured as an indicator of illite crystallinity (Weaver 1960). For each oriented powder sample of <2 μm size fraction, diffracted X-ray intensity was counted for 10 s five times at 10 Å, 10.5 Å and the background position, respectively, and the sharpness ratio was calculated from their mean values.

RESULTS AND OBSERVATIONS

Radiolarian strains

The calculated radiolarian strain ellipsoids are shown on a logarithmic Flinn graph (Fig. 3). Orientations of principal strain axes are plotted in Fig. 4. For each strain ellipsoid, the strain ellipsoid shape parameter K and the strain magnitude parameter $\bar{\varepsilon}_s$ are calculated from the principal-plane strain ratios:

$$K = \frac{\ln R_{XY}}{\ln R_{YZ}} \quad \text{(Ramsay 1967)} \qquad (1)$$

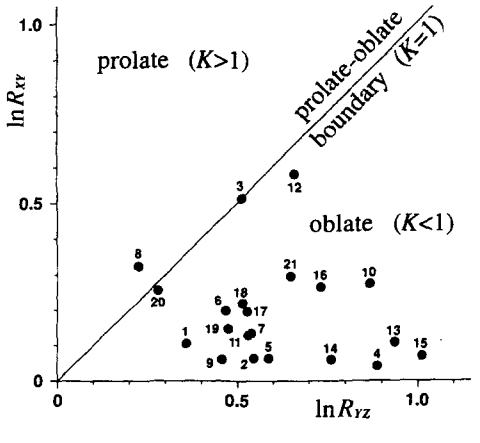

Fig. 3. Logarithmic Flinn plot of radiolarian strain ellipsoids. Numbers indicate their localities in Fig. 1.

$$\bar{\varepsilon}_s = \frac{1}{\sqrt{3}} \{(\ln R_{XY})^2 + (\ln R_{YZ})^2 + (\ln R_{XZ})^2\}^{1/2}$$

(Nadai 1963). (2)

The radiolarian strain ellipsoids vary in shape from uniaxially oblate to the prolate–oblate boundary of $K = 1$, with K values ranging from 0.05 to 1.44 (Fig. 3). $\bar{\varepsilon}_s$ values range from 0.34 to 0.88. No systematic change in K values with increasing strain magnitude is recognized.

Phyllosilicate basal plane fabrics

Pole figures obtained are shown in Fig. 4. A relatively weak intensity of illite/mica (004) peak compared with that of chlorite (002) resulted in a poor quality of the pole figures for illite/mica. Almost all pole figures for both chlorite and illite/mica are unimodal and exhibit orthorhombic symmetry, although several samples show slightly skewed pole figures (e.g. Fig. 4q). A systematic difference in the pattern of preferred orientation is recognized between chlorite and illite/mica. Chlorite pole figures are always more elongate than those of illite/mica, whereas illite/mica pole figures approximate to uniaxial clusters in most samples. In a few samples (e.g. Fig. 4h) long axes of elongate chlorite pole figures are approximately perpendicular to cleavage–bedding intersection (x axis), suggesting a possible contribution of a bedding-parallel fabric. However, in most samples there is no relation between the pattern of pole figures and cleavage–bedding intersection nor the orientation of bedding (triangles in Fig. 4), and therefore initial bedding fabric, if any, must not have significantly affected the final phyllosilicate basal plane fabrics.

Assuming that all pole figures are unimodal and have orthorhombic symmetry, they can be quantified using the orientation tensor method (the eigenvalue method of Woodcock 1977). The method was originally proposed by Scheidegger (1965) and Watson (1966) independently in order to find best-fit axes for girdle–cluster patterns of orientation data distributions. Its application to pole figure data was suggested by Cobbold & Gapais (1979). From normalized pole density $\rho(\alpha, \beta)$, where α and β represent tilt and azimuth angles, respectively, the orientation tensor **A** for each pole figure data is obtained by the following equation (Kanagawa & Yoshida 1988):

$$\mathbf{A} = \frac{1}{\int_0^{2\pi}\int_0^{\pi/2} \sin\alpha \, d\alpha \, d\beta} \begin{bmatrix} a_{11} & a_{12} & a_{13} \\ a_{21} & a_{22} & a_{23} \\ a_{31} & a_{32} & a_{33} \end{bmatrix}, \qquad (3)$$

where

$$a_{11} = \int_0^{2\pi}\int_0^{\pi/2} \rho(\alpha, \beta) \sin^3\alpha \cos^2\beta \, d\alpha \, d\beta \qquad (4)$$

$$a_{22} = \int_0^{2\pi}\int_0^{\pi/2} \rho(\alpha, \beta) \sin^3\alpha \sin^2\beta \, d\alpha \, d\beta \qquad (5)$$

$$a_{33} = \int_0^{2\pi}\int_0^{\pi/2} \rho(\alpha, \beta) \sin\alpha \cos^2\alpha \, d\alpha \, d\beta \qquad (6)$$

$$a_{12} = a_{21} = \int_0^{2\pi} \int_0^{\pi/2} \rho(\alpha, \beta) \sin^3\alpha \sin\beta \cos\beta \, d\alpha \, d\beta \quad (7)$$

$$a_{23} = a_{32} = \int_0^{2\pi} \int_0^{\pi/2} \rho(\alpha, \beta) \sin^2\alpha \sin\beta \cos\alpha \, d\alpha \, d\beta \quad (8)$$

$$a_{31} = a_{13} = \int_0^{2\pi} \int_0^{\pi/2} \rho(\alpha, \beta) \sin^2\alpha \cos\alpha \cos\beta \, d\alpha \, d\beta. \quad (9)$$

The eigenvectors $\mathbf{e}_1$, $\mathbf{e}_2$ and $\mathbf{e}_3$ of this tensor correspond to the best-fit orthogonal axes of a pole figure, and the eigenvalues E_1, E_2 and E_3 ($E_1 \geq E_2 \geq E_3$; $E_1 + E_2 + E_3 = 1$) characterize the pattern and strength of preferred orientation (Watson 1966, Woodcock 1977).

Each pole figure is plotted as a point on a logarithmic eigenvalue ratio graph (Fig. 5), which is analogous to the logarithmic Flinn graph. The graph used here is modified from that of Woodcock (1977) so that pole figure data can be applied. The pattern and strength of preferred orientation can be expressed by using the following parameters:

$$K_f = \frac{\ln(E_2/E_3)}{\ln(E_1/E_2)} \quad \text{(Woodcock 1977)} \quad (10)$$

$$\bar{\varepsilon}_f = \frac{1}{\sqrt{3}}[\{\ln(E_1/E_2)\}^2 + \{\ln(E_2/E_3)\}^2 + \{(\ln(E_1/E_3)\}^2]^{1/2} \quad \text{(Gapais \& Brun 1981)} \quad (11)$$

which are analogous to the strain ellipsoid shape parameter K and the strain magnitude parameter $\bar{\varepsilon}_s$, respectively (equations 1 and 2). K_f ranges from zero (uniaxial clusters) through unity (girdle–cluster transitions) to infinity (uniaxial girdles) (cf. Woodcock 1977, Woodcock & Naylor 1983).

All pole figures obtained in this study are clusters with low and narrow range of K_f values (Fig. 5). K_f values of chlorite pole figures range from 0.05 to 0.31, whereas those of illite/mica range from 0.01 to 0.13, indicating that illite/mica fabrics are closer to uniaxial clusters. $\bar{\varepsilon}_f$ values range from 1.49 to 2.44 in chlorite, and from 1.40 to 2.24 in illite/mica. There is no systematic difference in fabric strength ($\bar{\varepsilon}_f$ value) between chlorite and illite/mica. It should be noted here, however, that the phyllosilicate basal plane fabrics obtained in this study yield K_f values underestimated as well as $\bar{\varepsilon}_f$ values overestimated, although they yield correct eigenvectors (see Appendix; Figs. A1 and A2).

Comparison of phyllosilicate basal plane fabrics with radiolarian strains

On each pole figure in Fig. 4, eigenvectors $\mathbf{e}_1$, $\mathbf{e}_2$ and $\mathbf{e}_3$ of the calculated orientation tensor are shown together with principal axes X, Y and Z of radiolarian strain ellipsoids. In each pole figure there is a reasonably good, although not exact, coincidence of eigenvectors and principal strain axes. Eigenvector $\mathbf{e}_1$, which corresponds to the maximum eigenvalue E_1 and defines the cleavage-normal direction, is almost always parallel to Z axis which is the axis of minimum principal strain and defines the maximum shortening direction. Eigenvector $\mathbf{e}_3$, which corresponds to the minimum eigenvalue E_3 and defines the mineral lineation direction, is approximately parallel to the X axis which is the axis of maximum principal strain and defines the stretching direction. In several samples (e.g. Figs. 4b, c, e, r & u) there is a discrepancy in eigenvectors between chlorite and illite/mica, which results in a discrepancy between eigenvectors of either chlorite or illite/mica, the latter in most cases, and principal strain axes. Eigenvectors of illite/mica are less accurate than those of chlorite, because the former's pole figures are less precise and are close to uniaxial clusters with nearly equal E_1 and E_3 values.

Figure 6 is a plot of K_f values (abscissa) against the corresponding K values (ordinate). Although the K_f values of both chlorite and illite/mica obtained in this study are markedly smaller than the corresponding K values, the difference is partly due to the underestimation of K_f values. The K_f values of illite/mica are systematically smaller than those of chlorite.

A positive correlation exists between fabric strength ($\bar{\varepsilon}_f$) and strain magnitude ($\bar{\varepsilon}_s$) (Fig. 7). However, the scatter of data points indicates that the relationship is not so simple as to be represented by a single regression line passing through the origin. Fabric strength differences between chlorite and illite/mica also vary from sample to sample in no systematic way.

Microstructural observations

All slates studied in this study have a domainal microstructure consisting of cleavage domains (seams, films or P domains) and intercleavage domains (microlithons or Q domains) as seen in most cleaved rocks (e.g. Borradaile *et al.* 1982). These microstructures change as fabric strength increases, as described below.

In samples with relatively weak fabric strength ($\bar{\varepsilon}_f$ values for chlorite smaller than 1.78), embryonic and anastomosing cleavage domains are dark to opaque in appearance (Figs. 8a, c & e). Carbonaceous matter, sphene, ilmenite or rutile, apatite and epidote as well as phyllosilicates are concentrated in these cleavage domains (Figs. 8b, d & f). The concentration of carbonaceous matter and/or fine-grained sphene is especially characteristic of cleavage domains in these samples. They are particularly well concentrated in places where clastic quartz–feldspar grains or radiolarian skeletons are truncated by cleavage domains (Figs. 8c–f). Phyllosilicates (chlorite and illite and/or muscovite) are oriented subparallel to the cleavage trace in cleavage domains, whereas those in intercleavage domains are variously oriented.

As fabric strength increases, cleavage domains become transparent as well as parallel and continuous (Figs. 9a, c & e). They are composed mainly of phyllosilicates; carbonaceous matter, sphene, ilmenite, rutile, apatite and epidote are scattered and only locally concentrated (Figs. 9b, d & f). Phyllosilicates in both cleavage and intercleavage domains are well oriented

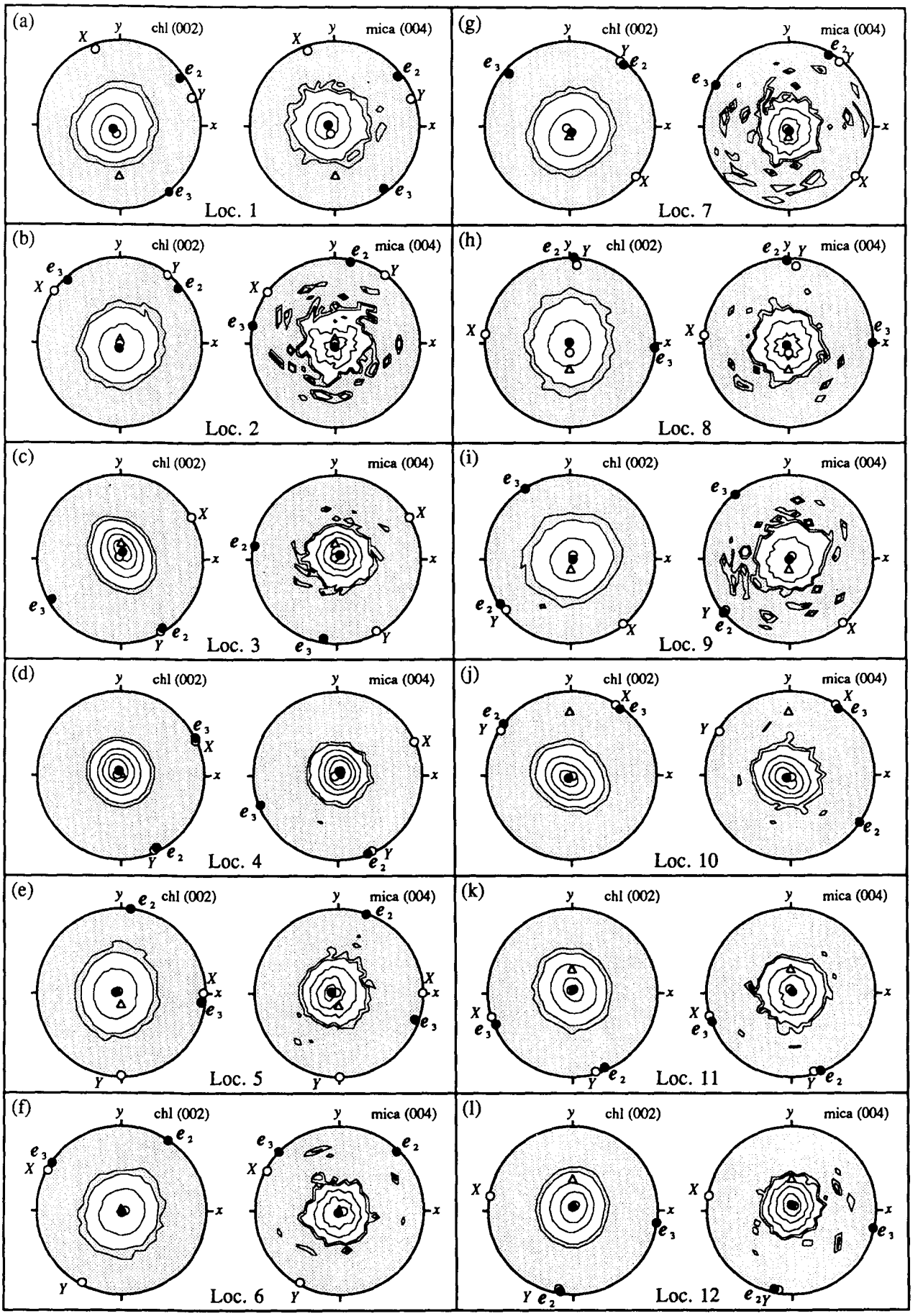

Fig. 4. Pole figures of chlorite (002) and illite/mica (004) basal planes. Lower-hemisphere equal-area projections. Contours at 0.5, 1, 5, 10, 15 and 20 in multiples of a random distribution density. Areas with pole densities less than the random distribution density (<1) are stippled. Pole figures are referred to specimen co-ordinates x and y (see Fig. 2). On each pole figure, pole of bedding (open triangle), principal axes of radiolarian strain ellipsoid (open circles), and eigenvectors of orientation tensor (closed circles) are shown. Principal strain axes X and Y, and eigenvectors $\mathbf{e}_2$ and $\mathbf{e}_3$ are indicated. The principal strain axis and eigenvector located in the center of pole figure represent Z and $\mathbf{e}_1$, respectively.

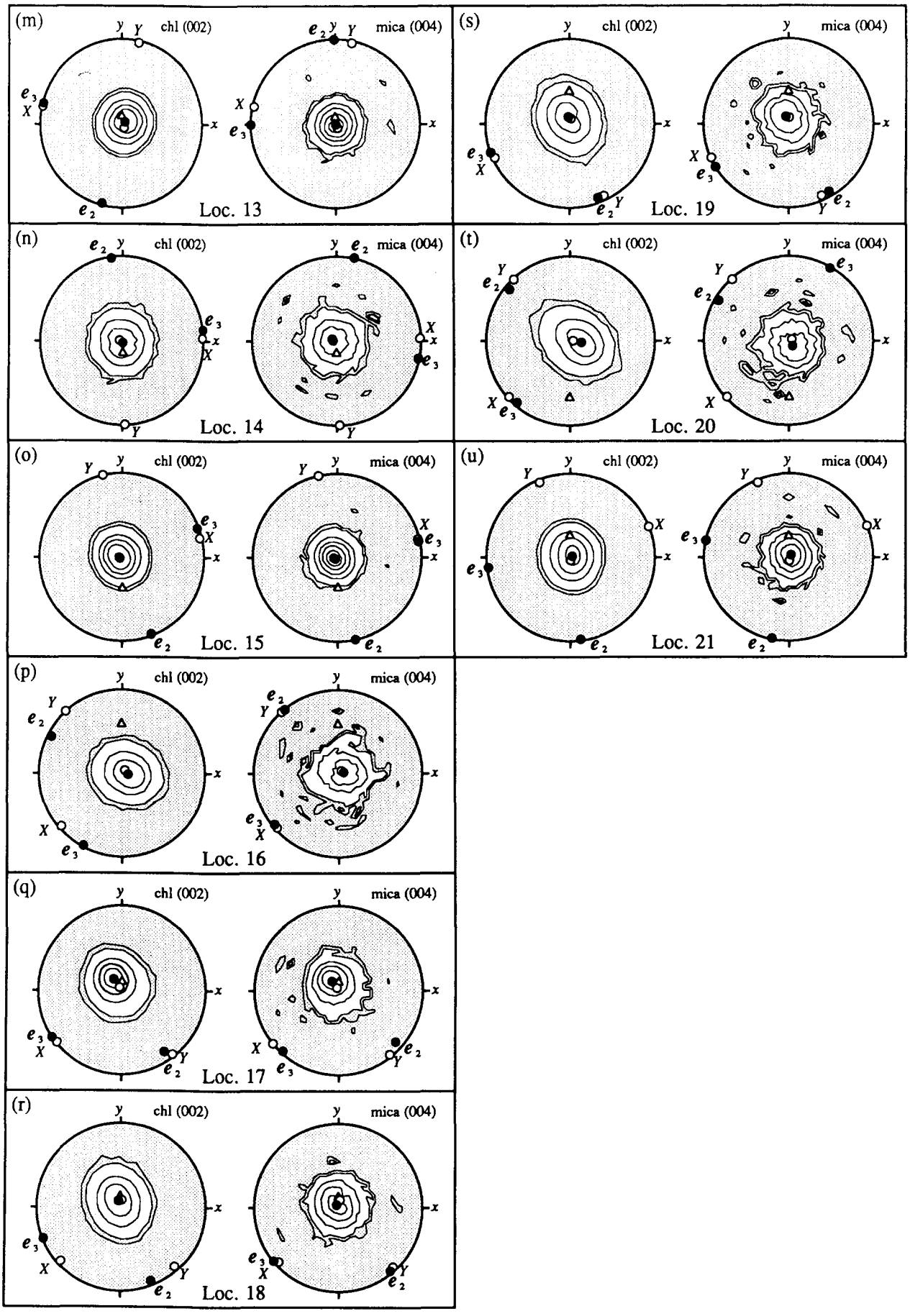

Fig. 4. *Continued.*

subparallel to the cleavage trace, except that large detrital grains are aligned with their basal planes parallel to bedding and show a slight bending (Figs. 9a & b). Phyllosilicates are more concentrated in cleavage domains than in intercleavage domains. As cleavage further develops, abundant well-oriented phyllosilicates obscure the domainal microstructure (Figs. 9e & f).

Grain size distribution of phyllosilicates

Both chlorite and illite/muscovite in samples with weak fabric strength show a wide range in grain size from 1 to 6 μm. They also show a low concentration in each sample (Fig. 10, localities 8 and 2). As fabric strength increases, they become finer-grained and more uniform in grain size ranging from 0.5 to 3 μm (localities 1 and 17). In samples with very strong fabric strength, phyllosilicates are 0.8–4 μm in grain size, showing a slight increase in average grain size (locality 21).

Whole-rock chemistry

Table 1 shows bulk chemical compositions of the studied slate samples, arranged according to the chlorite fabric strength. Although each element varies in concentration from sample to sample, the data show no systematic change in element concentrations in accordance with cleavage development. Wet chemical analyses of two Permian slate samples from the same area (Kambe *et al.* 1969) show no detectable CO_2 and carbon contents of 0.35 and 0.41%, which are roughly equivalent with the total carbon contents of 0.27–0.66% obtained in this study. Total carbon contents obtained here may represent organic carbon.

Illite crystallinity

The Weaver Index of illite crystallinity (sharpness ratio) ranges in the studied samples from 7.6 to 12.0. A plot of fabric strength ($\bar{\varepsilon}_f$ value) against sharpness ratio is shown in Fig. 11. Data points clearly display a positive correlation between fabric strength and illite crystallinity, and therefore suggest that cleavage develops with increasing metamorphic grade.

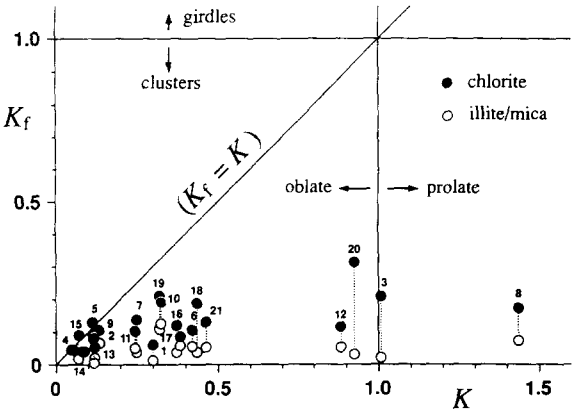

Fig. 6. Plot of fabric pattern parameters (K_f) of chlorite and illite/mica against shape parameter (K) of radiolarian strain ellipsoid. Plots for chlorite and illite/mica from the same sample are connected by a dotted line. Numbers indicating sample localities are given near the chlorite data points.

DISCUSSION

Difference in basal plane fabrics between chlorite and illite/mica

A systematic difference exists between the phyllosilicate basal plane fabrics of chlorite and illite/mica. The K_f values of illite/mica are consistently smaller than those of chlorite, indicating that illite/mica fabrics are closer to uniaxial clusters than chlorite fabrics (Figs. 4, 5 and 6). This tendency holds irrespective of measurement techniques (Figs. A1 and A2). In fabric strength, there is no significant difference between chlorite and illite/mica, although their $\bar{\varepsilon}_f$ values differ in the same samples (Figs. 5 and 7).

Differences in basal plane fabrics between chlorite and illite/mica have been reported by several authors.

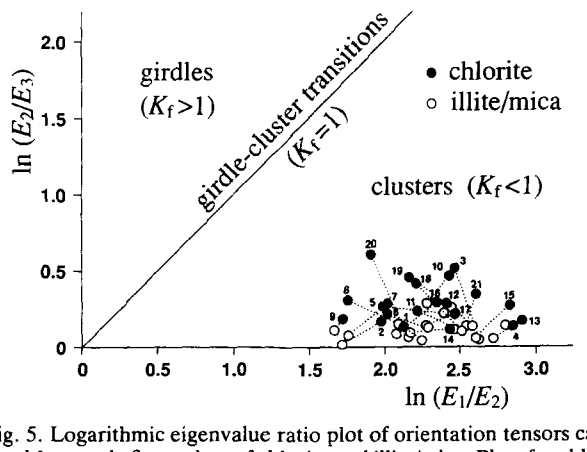

Fig. 5. Logarithmic eigenvalue ratio plot of orientation tensors calculated from pole figure data of chlorite and illite/mica. Plots for chlorite and illite/mica from the same sample are connected by a dotted line. Numbers indicating sample localities are given near the chlorite data points.

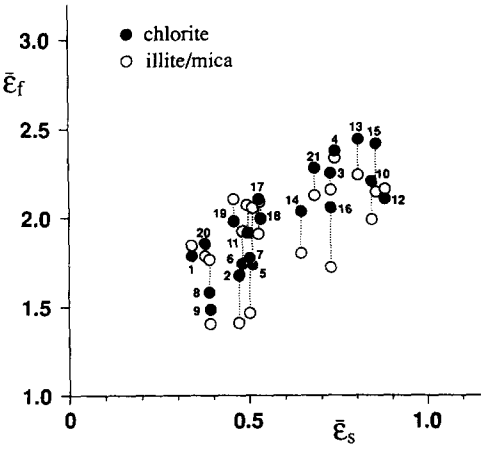

Fig. 7. Plot of fabric strength parameter ($\bar{\varepsilon}_f$) of chlorite and illite/mica against strain magnitude parameter ($\bar{\varepsilon}_s$) of radiolarian strain ellipsoid. Plots for chlorite and illite/mica from the same sample are connected by a dotted line. Numbers indicating sample localities are given near the chlorite data points.

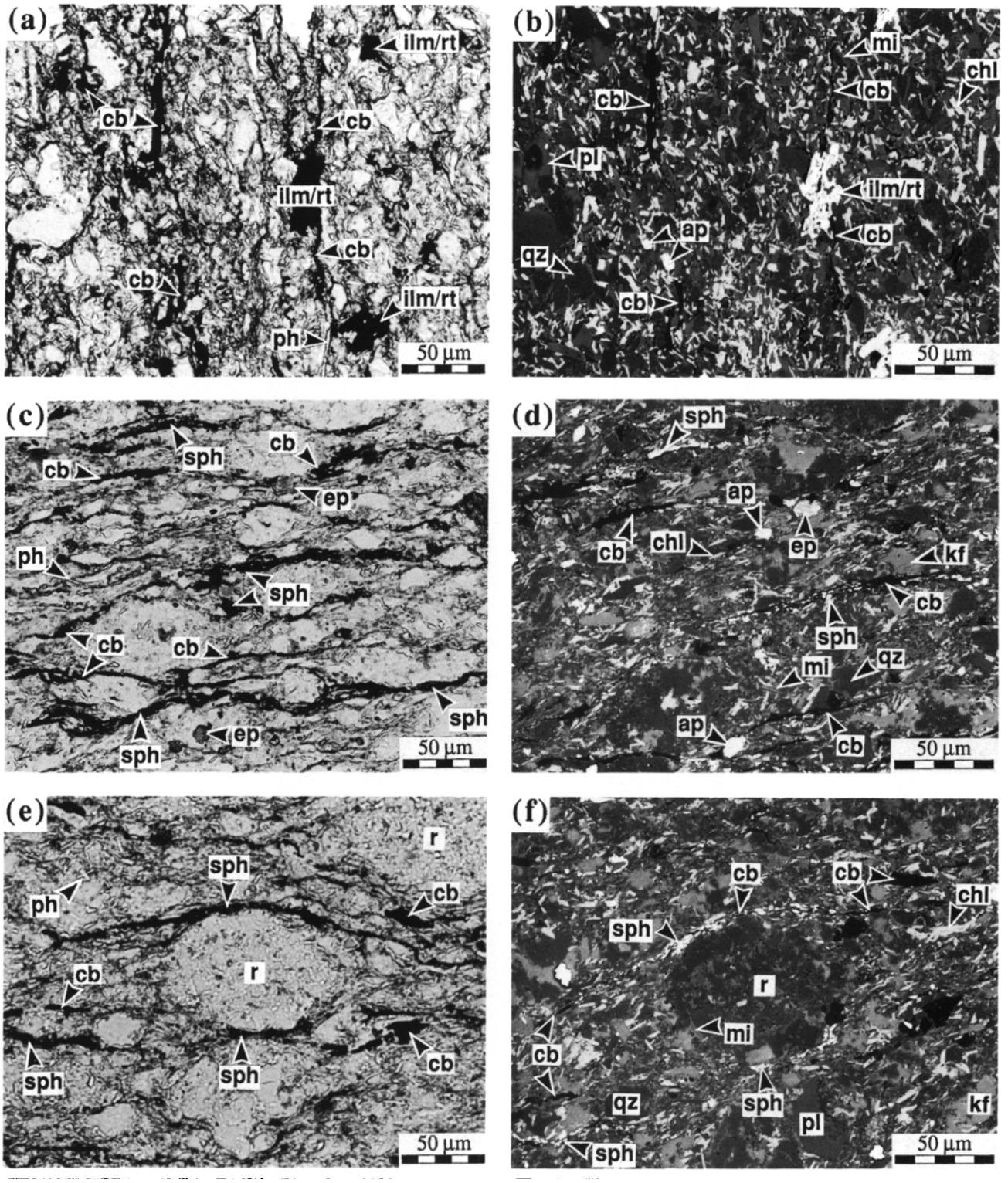

Fig. 8. Optical and BSE micrographs illustrating microstructures in slates with relatively weak fabric strength. Each BSE micrograph on the right covers the same but slightly smaller area of the optical micrograph in plane polarized light on the left. Samples are from locality 8 for (a) and (b), and from locality 2 for (c)–(f). ap = apatite; cb = carbonaceous matter (black in BSE micrograph); chl = chlorite (light grey); ep = epidote; ilm/rt = composite grain of ilmenite and rutile; kf = K-feldspar; mi = illite/muscovite (dark grey); ph = phyllosilicate; pl = plagioclase; qz = quartz; r = radiolarian skeleton; sph = sphene.

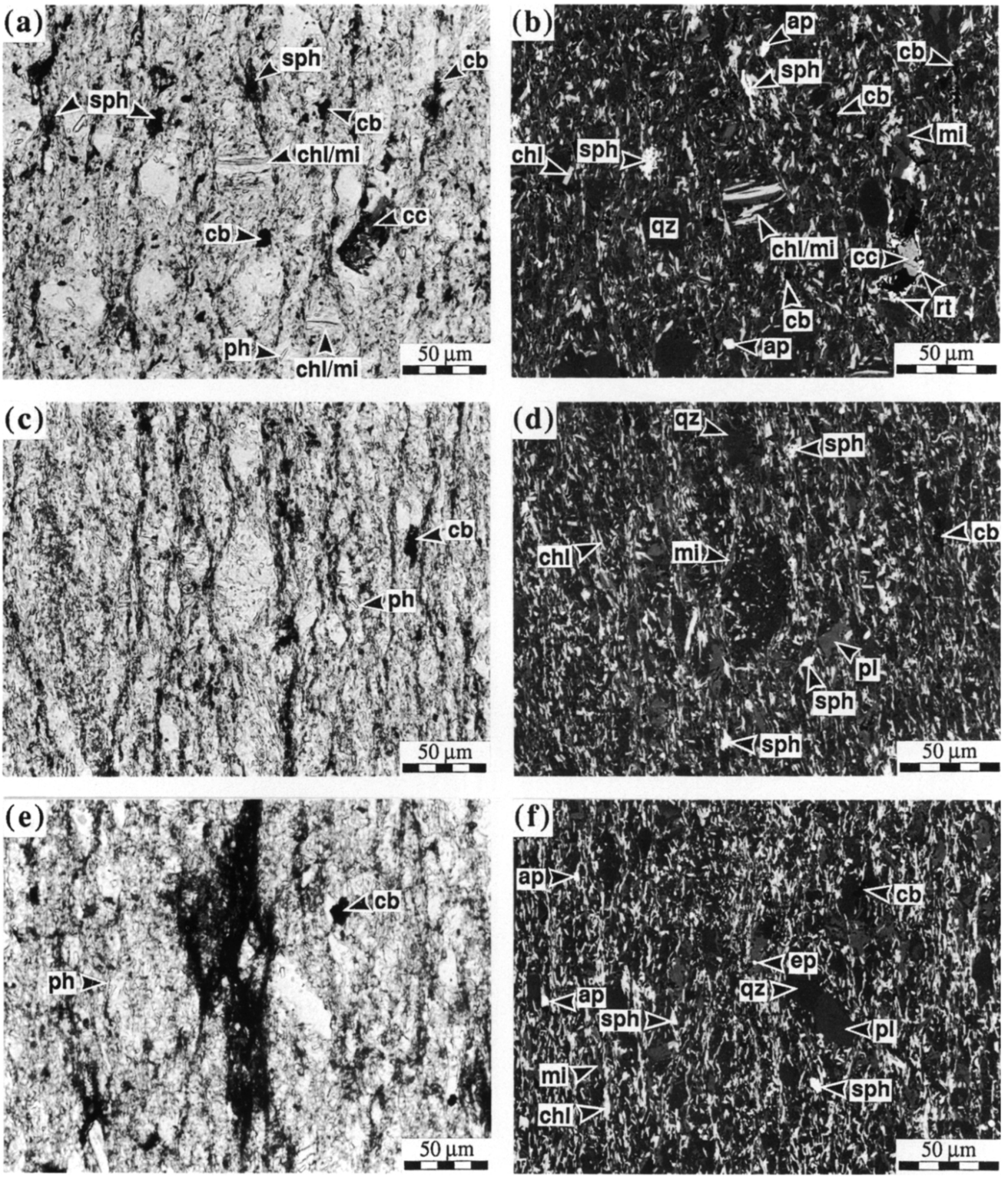

Fig. 9. Optical (left) and BSE (right) micrographs illustrating microstructures in slates with relatively strong fabric strength. Samples are from locality 1 for (a) and (b), from locality 17 for (c) and (d), and from locality 21 for (e) and (f). cc = calcite; chl/mi = composite grain of chlorite and muscovite; rt = rutile. Other abbreviations are the same as in Fig. 8.

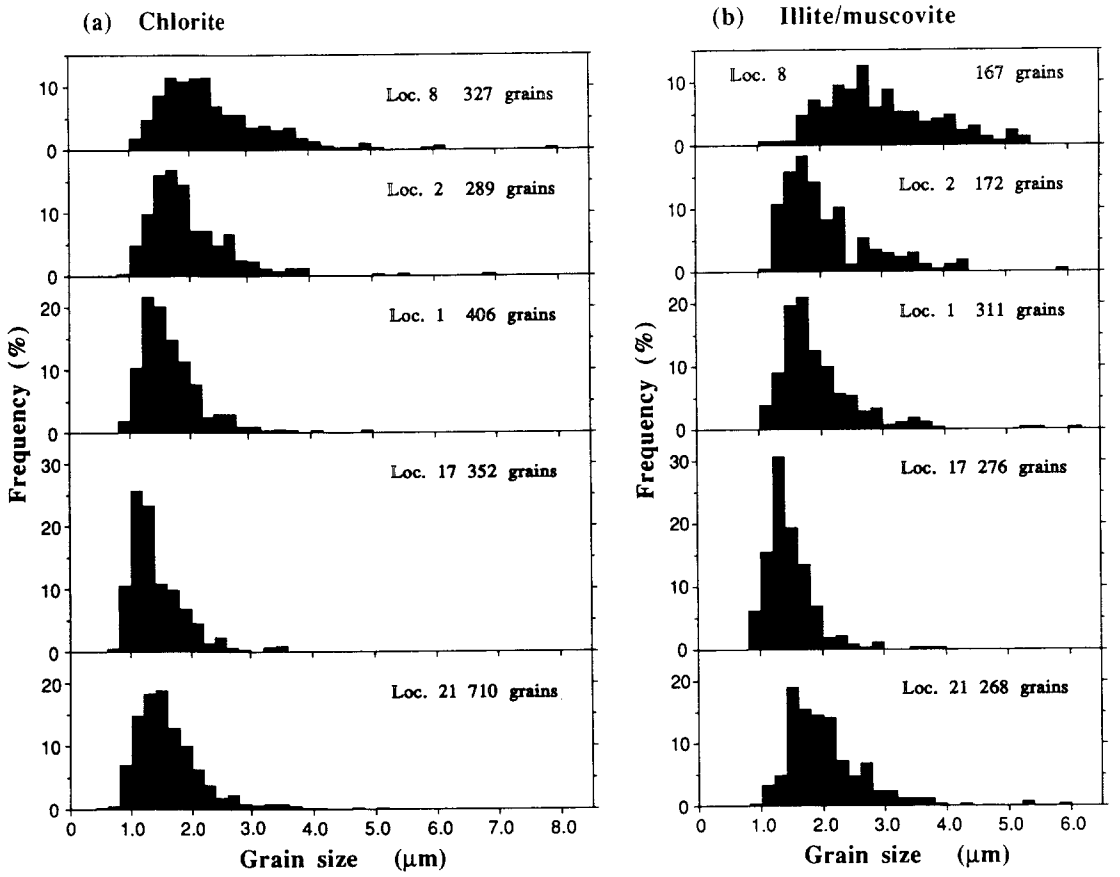

Fig. 10. Grain size distributions of (a) chlorite and (b) illite/muscovite in five slate samples, obtained from BSE micrographs.

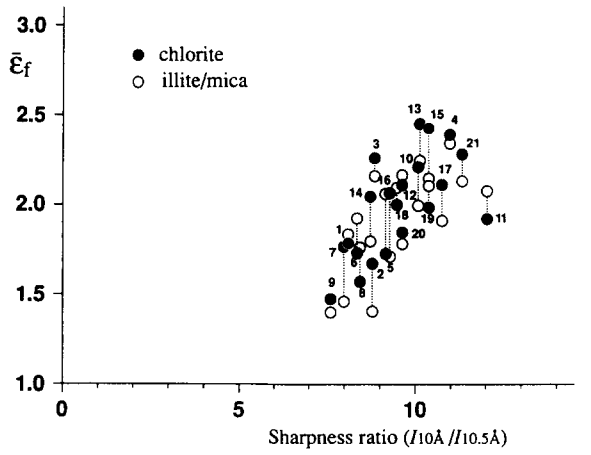

Fig. 11. Plot of fabric strength parameter ($\bar{\varepsilon}_f$) against sharpness ratio of 10 Å illite/mica peak (Weaver Index of illite crystallinity). Plots for chlorite and illite/mica from the same sample are connected by a dotted line. Numbers indicating sample localities are given near the chlorite data points.

Siddans (1976, 1977) noted that maximum pole densities of muscovite are consistently higher than those of chlorite in slates of the French Alps, North Wales and English Lake District. In contrast, Le Corre (1979), using the weighted orientation tensor method (Cobbold & Gapais 1979), showed that chlorite fabrics in slates of Central Brittany are consistently stronger than muscovite without significant difference in K_f values. He ascribed the difference to the fact that there are abundant sedimentary mica grains whereas most chlorite grains crystallized during metamorphism. Differences in fabric pattern between chlorite and illite/mica have been reported from Martinsburg slates by Holeywell & Tullis (1975), from slates of Rheinisches Schiefergebirge by Weber (1981), and from Kitakami slates by Ishii (1988a). These differences have been attributed to the presence of abundant chlorite porphyroblasts (Weber 1981, Woodland 1982) or large detrital mica grains (Ishii 1988a), which skew the pole figures away from the cleavage poles (Etheridge & Oertel 1979, Weber 1981, Ishii 1988a). In summary, the differences in basal plane fabrics between the two mineral species reported hitherto are mainly attributed to differing abundance of the two minerals either of primary or secondary origin.

9 The difference in basal plane fabrics revealed in this study is not similar to any of those mentioned above. It is not a difference in fabric strength nor in fabric pattern skewness. Basal plane fabrics of both minerals are not apparently affected by bedding fabric because pole figures in most samples are unrelated to the orientation of bedding (Fig. 4). Instead, only the K_f values are different for chlorite and illite/mica, suggesting distinct behavior during cleavage development. The nature of this difference is uncertain at present and remains to be further studied. Ishii (1988a) revealed a difference in mode of grain coarsening between the two mineral species through metamorphism and suggested a difference in thermodynamic character of these minerals. Such an intrinsic difference between the two mineral species, e.g.

the difference in anisotropy of growth rate, may be responsible for the observed difference in fabric pattern.

Relationships between phyllosilicate basal plane fabrics and radiolarian strains

A limited number of studies have compared phyllosilicate basal plane fabrics with finite strains in naturally deformed rocks (Oertel 1970, Tullis & Wood 1975, Siddans 1976, 1977, Wood & Oertel 1980, Gapais & Brun 1981, Oertel *et al.* 1989). The results include (1) reasonable coincidence between principal axes of fabric and those of finite strain, and (2) positive correlation between fabric strength and finite strain magnitude. Although both of these had already been recognized by the end of the last century (Siddans 1972, Wood 1974), they are also verified in this study (Figs. 4 and 7).

Oertel (1978, 1983) stated that "strain calculated according to March from the preferred orientation of phyllosilicate is *in many cases nearly the same* as strain measured by completely independent methods". However, no good correlation has been obtained in any previous studies except that of Wood & Oertel (1980) who deduced correlation parameters between finite strains determined from reduction spots and March strains calculated from muscovite preferred orientations. These are applicable only for the Cambrian slates of Wales.

The phyllosilicate basal plane fabrics obtained in this study differ from those predicted from the March model in the following two points: (1) the difference in fabric pattern between chlorite and illite/mica which would not exist according to the model; and (2) the possible difference between strain ellipsoid shape and fabric pattern. Numerical simulation studies according to the March model (Cobbold & Gapais 1979, Harvey & Laxton 1980, Sanderson & Meneilly 1981) indicate that K_f values of phyllosilicate fabrics should be generally larger (smaller in their papers because of reversed co-ordinates) than the corresponding K values. However, K_f values of both chlorite and illite/mica are probably smaller than the corresponding K values (Fig. 6). Gapais & Brun (1981) showed a similar relationship between biotite fabrics and finite strains in amphibolites of Finland. However, there may not be a significant difference between phyllosilicate fabric pattern and bulk strain ellipsoid shape because of the following two reasons. First the K_f values obtained in this study are underestimated and do not represent true phyllosilicate fabric patterns. Secondly, the radiolarian strain ellipsoids are probably more prolate than the bulk strain ellipsoids due to the viscosity contrast between radiolarians and their matrix (cf. Freeman & Lisle 1987, Treagus 1988). Their relationship therefore needs to be further studied.

Dominant mechanisms for phyllosilicate preferred orientation

Carbonaceous matter, sphene, ilmenite, rutile, apatite and epidote as well as phyllosilicates, which are

Table 1. Bulk chemical compositions of studied slate samples which are arranged according to the chlorite fabric strength. Values are expressed as weight percent

Sample No.	9	8	2	6	5	7	1	20	11	19	18	14	16	12	17	10	3	21	4	15	13
SiO_2	63.26	61.77	63.95	62.20	60.89	62.87	63.71	64.06	61.83	59.93	64.46	64.74	66.65	58.55	71.20	68.41	61.76	63.46	63.43	62.81	59.08
Al_2O_3	17.71	19.04	16.67	17.82	19.73	16.85	18.64	17.08	18.61	18.06	18.18	15.93	14.76	19.61	12.97	16.48	18.64	17.51	18.30	17.15	18.52
TiO_2	0.98	0.95	0.74	0.86	1.00	0.93	0.68	0.80	1.11	0.88	0.71	0.74	0.73	1.12	0.53	0.80	0.97	0.85	1.15	0.85	1.08
Fe_2O_3*	8.02	7.90	5.73	8.78	8.45	9.76	5.42	6.67	7.44	8.09	6.47	5.44	6.36	10.61	6.02	4.49	8.81	7.57	6.66	7.48	9.60
MgO	2.06	2.21	2.20	2.52	2.21	2.81	2.07	2.39	1.93	2.72	2.40	2.20	2.17	2.47	2.04	1.34	2.16	2.55	1.61	2.51	2.17
MnO	0.04	0.07	0.05	0.10	0.08	0.07	0.09	0.08	0.07	0.07	0.07	0.05	0.07	0.13	0.11	0.02	0.08	0.09	0.09	0.09	0.10
CaO	1.03	1.28	0.96	1.57	1.20	1.11	0.78	1.00	0.78	0.99	0.99	0.38	2.05	0.85	0.82	1.77	0.98	1.03	0.92	0.85	1.61
Na_2O	1.11	2.64	1.46	2.36	2.36	1.93	1.75	2.91	2.59	2.70	2.57	3.49	2.55	3.74	1.81	1.61	0.95	2.80	2.22	2.63	2.91
K_2O	2.03	2.04	5.51	1.47	2.16	1.38	3.34	2.18	2.36	2.15	2.43	2.33	1.48	1.54	1.83	1.19	2.08	2.10	2.26	2.11	1.62
P_2O_5	0.05	0.10	0.12	0.12	0.10	0.07	0.14	0.14	0.09	0.14	0.13	0.15	0.14	0.10	0.08	0.05	0.06	0.17	0.07	0.17	0.08
C†	0.36	0.52	0.66	0.47	0.53	0.61	0.51	0.29	0.50	0.46	0.31	0.52	0.46	0.27	0.30	0.65	0.46	0.33	0.45	0.29	0.32
Total	96.65	98.52	98.05	98.27	98.71	98.39	97.13	97.60	97.31	96.19	98.72	95.97	97.42	98.99	97.71	97.11	96.95	98.46	97.16	96.94	97.09

* Total iron as Fe_2O_3.
† Total contents of organic and carbonate carbons determined by using a carbon determinator. Other elements are determined by X-ray fluorescence analysis.

concentrated in cleavage domains in slates with relatively weak fabric strength (Fig. 8), are typically regarded as insoluble residues (Durney 1972, Williams 1972, Nickelsen 1972, 1979, Groshong 1975, 1976, Alvarez *et al.* 1976, Gray 1977, 1978, 1979, 1981, Borradaile *et al.* 1982, Woodland 1982, Wright & Platt 1982). Preferred orientation of phyllosilicates in cleavage domains, as well as concentration of these insoluble residues, strongly suggest that pressure solution transfer is dominant in these slates. Although pressure solution transfer is not a direct mechanism for phyllosilicate preferred orientation, it results in passive reorientation of phyllosilicate grains into solution surfaces (i.e. cleavage domains) as matrix minerals are removed.

In contrast, phyllosilicates in slates with relatively strong fabric strength show rather uniform grain size and subparallel orientation in cleavage and intercleavage domains (Fig. 10, localities 1 and 17; Figs. 9a–d), suggesting crystallization or recrystallization through metamorphism. Crystallization or recrystallization under non-hydrostatic stress is accompanied with oriented nucleation or oriented growth of phyllosilicates, which result in their preferred orientation. Dense concentration of phyllosilicates in cleavage domains (Fig. 9) may be the result of pressure solution transfer during the earlier stage and later enhancement by crystallization–recrystallization. Scattered occurrences of insoluble residues implies that they are partly broken down by metamorphic reactions. In slates with even greater fabric strength, abundant well-oriented phyllosilicates diffuse the domainal structure (Figs. 9e & f). A slight increase of grain size (Fig. 10, locality 21) indicates the coarsening of phyllosilicate grains.

These lines of microstructural evidence suggest that the dominant mechanism for phyllosilicate preferred orientation in the slates studied here changes as cleavage develops from pressure solution transfer, through syntectonic crystallization–recrystallization, and possibly to oriented grain growth.

No evidence was found in this study that mechanical rotation was dominant during cleavage development. Previous studies have revealed that mechanical rotation accompanying microcrenulation can play an important role during an early stage of cleavage development in slates with a strong initial phyllosilicate preferred orientation (Williams 1972, Cosgrove 1976, Gray 1977, 1978, 1979, 1981, Roy 1978, White & Knipe 1978, Knipe 1981, Weber 1981, White & Johnston 1981). In such slates, grain boundary sliding can accommodate microcrenulation (Cosgrove 1976, Gray 1979, 1981, Knipe 1981, Weber 1981). Because mechanical rotation is a strain-hardening process, there would be a limit of strain above which it becomes less effective due to mutual grain interference (Tullis 1976). Thus mechanical rotation would be expected to be followed by strain-softening processes such as pressure solution transfer or syntectonic crystallization and/or recrystallization (Gray & Durney 1979). In slates without strong initial fabrics, mechanical rotation may be less important throughout cleavage development because grain boundary sliding is inhibited (Woodland 1982). This seems to be also the case for slates in this study. Mutual grain interference seems to have prevented mechanical rotation of phyllosilicates at fairly small strains so that mechanical rotation may have been dominant only at very small strains.

Factors affecting the dominance of preferred orientation mechanisms

The observation that phyllosilicate fabric strength increases with increasing metamorphic grade, as represented by illite crystallinity, was also reported by Siddans (1977), Weber (1981) and Ishii (1988a). Illite crystallinity in slates of the Kitakami Mountains mainly reflects the thermal effect of Early Cretaceous granites (Ishii 1988a,b). Illite crystallinity variation is therefore considered to imply a variation of metamorphic temperature. The change in dominant mechanisms for phyllosilicate preferred orientation with increasing fabric strength thus suggests that metamorphic temperature must be one of the major factors which control the dominance of phyllosilicate preferred orientation mechanisms.

In crenulation cleavage development, cleavage fabric initiates as microcrenulation which is followed by pressure solution and syntectonic crystallization or grain growth as metamorphic temperature increases (Gray & Durney 1979, Weber 1981). Ishii (1988a) emphasized a threshold metamorphic grade above which grain coarsening and preferred orientation of phyllosilicates are abruptly advanced mainly due to oriented grain growth. Grain coarsening did not occur to a significant degree in the slates studied; the phyllosilicates probably first became finer-grained due to crystallization or recrystallization through metamorphic reactions, then they became slightly coarser-grained probably due to oriented grain growth (Fig. 10). Ishii (1988a) plotted fabric strength (chlorite maximum pole density) against illite crystallinity (Kubler Index) (fig. 9 in Ishii 1988a). Fabric strength does not increase below a threshold value of illite crystallinity whereas it increases abruptly above the value. His results are similar to those in this study except that no threshold value of illite crystallinity was found in this study (Fig. 11). His threshold value of illite crystallinity (Kubler Index value of 0.29) corresponds to the Weaver Index value of about 4.5 (Weaver 1984), which is lower than all values of illite crystallinity obtained in this study. It is possible that mechanical rotation may have been active below this threshold metamorphic temperature. A possible path of dominant mechanisms in the Kitakami slates is illustrated in fabric strength–temperature space in Fig. 12.

Temperature increase under non-hydrostatic stress promotes pressure solution transfer and crystallization–recrystallization of phyllosilicates leading to slaty cleavage development, because these are thermally activated processes (Durney 1976, Rutter 1976). Temperature increase enables rocks to yield further strains which may also induce solution transfer and dynamic recrystalliza-

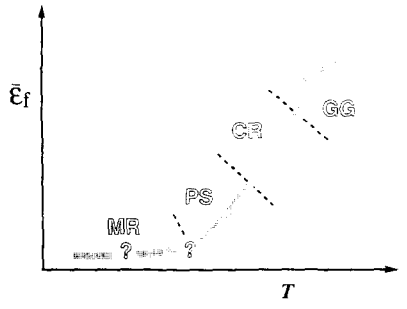

Fig. 12. Possible path of dominant mechanisms for phyllosilicate preferred orientation during cleavage development in the Kitakami slates. MR = mechanical rotation; PS = pressure solution transfer; CR = syntectonic crystallization–recrystallization; GG = oriented grain growth.

tion of minerals (e.g. Nicolas & Poirier 1976). Thus fabric strength and strain are not independent.

It is supposed that pressure solution transfer also dominates under lower stresses and lower strain rates, whereas syntectonic crystallization–recrystallization dominate under higher stresses and higher strain rates (Stocker & Ashby 1973, Rutter 1976, Gray & Durney 1979). Effects of stress and strain rate on the dominance of phyllosilicate preferred orientation mechanisms, however, remain uncertain.

Slaty cleavage development in the samples studied is apparently not affected by bulk chemical composition (Table 1). This is also the case for the Martinsburg slates at Lehigh Gap of Pennsylvania (Lee *et al.* 1986). These two cases are not consistent with the results of other studies. Le Corre (1977) and Weaver (1984) showed a decrease of such elements as SiO_2 and Na_2O as metamorphic grade increases. Gray (1977, 1981), Stephens *et al.* (1979) and Sutton (1989) revealed systematic differences in chemistry between cleavage and intercleavage domains. Knipe (1979, 1981), White & Johnston (1981), and Lee *et al.* (1984) revealed differences in phyllosilicate chemistry between cleavage and intercleavage domains. All of these are considered to be indirect evidence for pressure solution transfer or metamorphic crystallization–recrystallization. Such chemical variation should be also expected in the slates in this study. Lee *et al.* (1986) gave a possible explanation for Martinsburg slates at Lehigh Gap that solution flow, by which dissolved mass is transferred and from which new crystals precipitate, was not pervasive on the scale of the outcrop. The scale on which mass transfer and metamorphic reactions occurred may have not been beyond that of the hand specimen so that the slate samples in this study can be regarded as a closed system. However, it is difficult to interpret only with bulk major element data, and more detailed chemical analyses of the slates studied are needed.

CONCLUSIONS

(1) Phyllosilicate basal plane fabrics of selected slates from the Kitakami Mountains reveal that illite/mica fabrics are consistently closer to uniaxial clusters than chlorite fabrics in spite of no significant differences in fabric strength between them.

(2) Although phyllosilicate fabric strength has a positive correlation with radiolarian strain magnitude, there is a possible difference between fabric pattern and radiolarian strain ellipsoid shape, as well as a difference in fabric pattern between chlorite and illite/mica. Strain estimation from phyllosilicate basal plane fabrics based on the March model may be therefore unreliable unless their relationship is established in each case.

(3) Microstructures in the slates studied suggest that the dominant mechanism for phyllosilicate preferred orientation changes as cleavage develops from pressure solution transfer, through syntectonic crystallization–recrystallization, and possibly to oriented grain growth. Mechanical rotation seems to be of minor importance during cleavage development observed here, but it may have been active during the earlier stage.

(4) Because phyllosilicate basal plane fabrics and radiolarian strain tend to increase in strength and magnitude in accordance with increasing illite crystallinity, metamorphic grade (mainly temperature) must be one of the major factors which control the dominance of phyllosilicate preferred orientation mechanisms.

Acknowledgements—I thank Toshihiko Shimamoto for useful discussion, Michael Williams and James Pickens for comments on an earlier version of the manuscript, Ryuji Tada for advice during sample preparations for XRF, XRD and carbon analyses, and Hideto Yoshida for assisting with XRF and SEM analyses. Helpful reviews by an anonymous referee and Gerhard Oertel, and additional comments on measurement techniques of X-ray texture goniometry by Gerhard Oertel are gratefully acknowledged. This study was supported by grants 61420015, 62740455, and a research abroad grant from the Ministry of Education, Science and Culture of Japan.

REFERENCES

Agar, S. M., Prior, D. J. & Behrmann, J. H. 1989. Back-scattered electron imagery of the tectonic fabrics of some fine-grained sediments: Implications for fabric nomenclature and deformation processes. *Geology* **17**, 901–904.

Alvarez, W., Engelder, T. & Lowrie, W. 1976. Formation of spaced cleavage and folds in brittle limestone by dissolution. *Geology* **4**, 698–701.

Borradaile, G. J., Bayly, M. B. & Powell, C. McA. (editors) 1982. *Atlas of Deformational and Metamorphic Rock Fabrics*. Springer, Berlin.

Chen, R. T. & Oertel, G. 1989. Strain history of the Los Prietos syncline, Santa Maria basin, California: a case of post-tectonic compaction. *J. Struct. Geol.* **11**, 539–551.

Clark, B. R. 1970. Mechanical formation of preferred orientation in clay. *Am. J. Sci.* **269**, 250–266.

Cobbold, P. R. & Gapais, D. 1979. Specification of fabric shapes using an eigenvalue method: Discussion. *Bull. geol. Soc. Am.* **90**, 310–312.

Cosgrove, J. W. 1976. The formation of crenulation cleavage. *J. geol. Soc. Lond.* **132**, 155–178.

Dunnet, D. & Siddans, A. W. B. 1971. Non random sedimentary fabrics and their modifications by strain. *Tectonophysics* **12**, 307–325.

Durney, D. W. 1972. Solution-transfer, an important geological deformation mechanism. *Nature* **235**, 315–317.

Durney, D. W. 1976. Pressure-solution and crystallization deformation. *Phil. Trans. R. Soc. Lond.* **A283**, 229–240.

Ehiro, M., Okami, K. & Kanisawa, S. 1988. Recent progress and further subjects in studies on the "Hayachine Tectonic Belt" in the Kitakami Massif, Northeast Japan. *Earth Sci.* **42**, 317–335.*

Etheridge, M. A. & Lee, M. F. 1975. Microstructure of slates from Lady Loretta, Queensland, Australia. *Bull. geol. Soc. Am.* **86**, 13–22.

Etheridge, M. A. & Oertel, G. 1979. Strain measurements from phyllosilicate preferred orientation—a precautionary note. *Tectonophysics* **60**, 107–120.

Etheridge, M. A., Paterson, M. S. & Hobbs, B. E. 1974. Experimentally produced preferred orientation in synthetic mica aggregates. *Contr. Miner. Petrol.* **44**, 275–294.

Freeman, B. & Lisle, R. J. 1987. The relationship between tectonic strain and the three-dimensional shape fabrics of pebbles in deformed conglomerates. *J. geol. Soc. Lond.* **144**, 635–639.

Gapais, D. & Brun, J.-P. 1981. A comparison of mineral grain fabrics and finite strain in amphibolites from eastern Finland. *Can. J. Earth Sci.* **18**, 995–1003.

Gray, D. R. 1977. Differentiation associated with discrete crenulation cleavages. *Lithos* **10**, 89–101.

Gray, D. R. 1978. Cleavages in deformed psammitic rocks from southeastern Australia: Their nature and origin. *Bull. geol. Soc. Am.* **89**, 577–590.

Gray, D. R. 1979. Microstructure of crenulation cleavages: an indicator of cleavage origin. *Am. J. Sci.* **279**, 97–128.

Gray, D. R. 1981. Compound tectonic fabrics in singly folded rocks from southwest Virginia, U.S.A. *Tectonophysics* **78**, 229–248.

Gray, D. R. & Durney, D. W. 1979. Crenulation cleavage differentiation: implications of solution–deposition processes. *J. Struct. Geol.* **1**, 73–80.

Gregg, W. J. 1985. Microscopic deformation mechanisms associated with mica film formation in cleaved psammitic rocks. *J. Struct. Geol.* **7**, 45–56.

Groshong, R. H. 1975. Slip-cleavage caused by pressure solution in a buckle fold. *Geology* **3**, 411–413.

Groshong, R. H. 1976. Strain and pressure solution in the Martinsburg slate, Delaware Water Gap, New Jersey. *Am. J. Sci.* **276**, 1131–1146.

Harvey, P. K. & Laxton, R. R. 1980. The estimation of finite strain from the orientation of passively deformed linear markers: eigenvalue relationships. *Tectonophysics* **70**, 285–307.

Holeywell, R. C. & Tullis, T. E. 1975. Mineral reorientation and slaty cleavage in the Martinsburg Formation, Lehigh Gap, Pennsylvania. *Bull. geol. Soc. Am.* **86**, 1296–1304.

Ikeda, Y. 1984. Study on the Early Cretaceous tectonic movement in the Southern Kitakami Massif, Northeast Japan. *Geol. Rep. Hiroshima Univ.* **24**, 99–157.*

Ishii, K. 1985. Development of fold and slaty cleavage in the Oshika Peninsula, the South Kitakami Mountains. *J. geol. Soc. Jap.* **91**, 309–321.*

Ishii, K. 1988a. Grain growth and re-orientation of phyllosilicate minerals during the development of slaty cleavage in the South Kitakami Mountains, northeast Japan. *J. Struct. Geol.* **10**, 145–154.

Ishii, K. 1988b. Development of slaty cleavage and emplacement of granitic bodies in the South Kitakami Mountains, Japan. *Tohoku Univ. Inst. Geol. Paleont. Contr.* **91**, 1–14.*

Kambe, N., Katada, M. & Ohmori, T. 1969. Chemical composition and sedimentary environment of the Permian Toyoma clayslates from the Southern Kitakami Terrain. *Bull. geol. Surv. Jap.* **20**, 1–11.*

Kanagawa, K. 1985. Effects of granite emplacement on the Early Cretaceous cleavage-related deformation in the Kitakami Mountains, Northeast Japan. Unpublished Ph.D. thesis, University of Tokyo.

Kanagawa, K. 1986. Early Cretaceous folding and cleavage in the Kitakami Mountains, analyzed in the Ofunato terrane. *J. geol. Soc. Jap.* **92**, 349–370.

Kanagawa, K. 1990. Automated two-dimensional strain analysis from deformed elliptical markers using an image analysis system. *J. Struct. Geol.* **12**, 139–143.

Kanagawa, K. & Yoshida, S. 1988. Utility of the orientation-tensor method for quantitative representation of preferred orientations of phyllosilicates and amphiboles measured with X-ray texture goniometer. *J. Fac. Sci. Univ. Tokyo* **21**, 447–465.

Kato, M. 1985. Paleozoic and Mesozoic strata of the Kitakami Mountains, Japan: An overview. *Mem. geol. Soc. Jap.* **25**, 19–29.*

Knipe, R. J. 1979. Chemical changes during slaty cleavage development. *Bull. Minéral.* **102**, 206–209.

Knipe, R. J. 1981. The interaction of deformation and metamorphism in slates. *Tectonophysics* **78**, 249–272.

Knipe, R. J. & White, S. H. 1977. Microstructural variation and axial plane cleavage around a fold.—A H. V. E. M. study. *Tectonophysics* **39**, 355–381.

Krinsley, D. H., Pye, K. & Kearsley, A. T. 1983. Application of backscattered electron microscopy in shale petrology. *Geol. Mag.* **120**, 109–114.

Le Corre, C. 1977. Dissolution et comportement du quartz dans un gradient de déformation avec schistosité. *Bull. Soc. géol. Fr.* **19**, 1109–1113.

Le Corre, C. 1979. L'évolution typologique et texturale des roches argilosilteuses au cours de la schistogenèse. Notion de trajectoire de fabrique. *Bull. Minéral.* **102**, 273–281.

Lee, J. H., Peacor, D. R., Lewis, D. D. & Wintsch, R. P. 1984. Chlorite–illite/muscovite interlayered and interstratified crystals: a TEM/AEM study. *Contr. Miner. Petrol.* **88**, 372–385.

Lee, J. H., Peacor, D. R., Lewis, D. D. & Wintsch, R. P. 1986. Evidence for syntectonic crystallization for the mudstone to slate transition at Lehigh Gap, Pennsylvania, U.S.A. *J. Struct. Geol.* **8**, 767–780.

March, A. 1932. Mathematische Theorie der Regelung nach der Korngestalt bei affiner Deformation. *Z. Kristalogr.* **81**, 285–297.

Means, W. D. 1975. Natural and experimental microstructures in deformed micaceous sandstones. *Bull. geol. Soc. Am.* **86**, 1221–1229.

Means, W. D. & Paterson, M. S. 1966. Experiments on preferred orientation of platy minerals. *Contr. Miner. Petrol.* **13**, 108–133.

Nadai, A. 1963. *Theory of Flow and Fracture of Solids*. McGraw-Hill, New York.

Nickelsen, R. P. 1972. Attributes of rock cleavage in some mudstones and limestones of the Valley and Ridge Province, Pennsylvania. *Penn. Acad. Sci. Proc.* **46**, 107–112.

Nickelsen, R. P. 1979. Sequence of structural stages of the Alleghany orogeny, at the Bear Valley Strip Mine, Shamokin, Pennsylvania. *Am. J. Sci.* **279**, 225–271.

Nicolas, A. & Poirier, J. P. 1976. *Crystalline Plasticity and Solid State Flow in Metamorphic Rocks*. John Wiley & Sons, London.

Oertel, G. 1970. Deformation of a slaty, lapillar tuff in the Lake District, England. *Bull. geol. Soc. Am.* **81**, 1173–1188.

Oertel, G. 1978. The development of slaty cleavage in a part of the French Alps—Discussion. *Tectonophysics* **47**, 185–187.

Oertel, G. 1983. The relationships of strain and preferred orientation of phyllosilicate grains in rocks—a review. *Tectonophysics* **100**, 413–447.

Oertel, G. 1985. Phyllosilicate textures in slates. In: *Preferred Orientation in Deformed Metals and Rocks: An Introduction to Modern Texture Analysis* (edited by Wenk, H.-R.). Academic Press, Orlando, 431–440.

Oertel, G., Engelder, T. & Evans, K. 1989. A comparison of the strain of crinoid columnals with that of their enclosing silty and shaly matrix on the Appalachian Plateau, New York. *J. Struct. Geol.* **11**, 975–993.

Oho, Y. 1982. Effective factors controlling cleavage formation and other microstructures in the South Kitakami Mountains. *J. Fac. Sci. Univ. Tokyo* **20**, 345–381.

Ozawa, K., Shibata, K. & Uchiumi, S. 1988. K–Ar ages of hornblende in gabbroic rocks from the Miyamori ultramafic complex of the Kitakami Mountains. *J. Jap. Ass. Miner. Petrol. Econ. Geol.* **83**, 150–159.*

Ramsay, J. G. 1967. *Folding and Fracturing of Rocks*. McGraw-Hill, New York.

Ramsay, J. G. & Huber, M. I. 1983. *The Technique of Modern Structural Geology, Volume* 1: *Strain Analysis*. Academic Press, London.

Roy, A. B. 1978. Evolution of slaty cleavage in relation to diagenesis and metamorphism: A study from the Hunsrückschiefer. *Bull. geol. Soc. Am.* **89**, 1775–1785.

Rutter, E. H. 1976. The kinetics of rock deformation by pressure solution. *Phil. Trans. R. Soc. Lond.* **A283**, 203–219.

Sanderson, D. J. & Meneilly, A. W. 1981. Analysis of three-dimensional strain modified uniform distributions: andalusite fabrics from a granite aureole. *J. Struct. Geol.* **3**, 109–116.

Scheidegger, A. E. 1965. On the statistics of the orientation of bedding planes, grain axes and similar sedimentological data. *Prof. Pap. U.S. geol. Surv.* **525C**, 164–167.

Shimamoto, T. & Ikeda, Y. 1976. A simple algebraic method for strain estimation from deformed ellipsoidal objects. 1. Basic theory. *Tectonophysics* **36**, 315–337.

Siddans, A. W. B. 1972. Slaty cleavage—a review of research since 1815. *Earth Sci. Rev.* **8**, 205–232.

Siddans, A. W. B. 1976. Deformed rocks and their textures. *Phil. Trans. R. Soc. Lond.* **A283**, 43–54.

Siddans, A. W. B. 1977. The development of slaty cleavage in a part of the French Alps. *Tectonophysics* **39**, 533–557.

Siddans, A. W. B. 1978. The development of slaty cleavage in a part of the French Alps—Reply. *Tectonophysics* **47**, 187–191.
Stephens, M. B., Glasson, M. S. & Keays, R. R. 1979. Structural and chemical aspects of metamorphic layering development in metasediments from Clunes, Australia. *Am. J. Sci.* **279**, 129–160.
Stocker, R. L. & Ashby, M. F. 1973. On the rheology of the upper mantle. *Rev. Geophys. & Space Phys.* **11**, 391–426.
Sutton, S. J. 1989. Orientation-dependent "metamorphic grade" in phyllosilicates belonging to a slaty cleavage fabric. *J. Geol.* **97**, 197–208.
Takizawa, F. 1981. Folding structures in the Mesozoic strata of the Ogatsu and Ojika areas, southern Kitakami Mountains—with a special reference to slaty cleavage. *Bull. Ass. Struct. Geol. Jap.* **26**, 43–57.†
Treagus, S. H. 1988. Strain refraction in layered systems. *J. Struct. Geol.* **10**, 517–527.
Tullis, T. E. 1976. Experiments on the origin of slaty cleavage and schistosity. *Bull. geol. Soc. Am.* **87**, 745–753.
Tullis, T. E. & Wood, D. S. 1975. Correlation of finite strain from both reduction bodies and preferred orientation of mica in slate from Wales. *Bull. geol. Soc. Am.* **86**, 632–638.
Watson, G. S. 1966. The statistics of orientation data. *J. Geol.* **74**, 786–797.
Weaver, C. E. 1960. Possible uses of clay minerals in search for oil. *Bull. Am. Ass. Petrol. Geol.* **44**, 1505–1518.
Weaver, C. E. 1984. *Shale–Slate Metamorphism in Southern Appalachians*. Elsevier, Amsterdam.
Weber, K. 1981. Kinetic and metamorphic aspects of cleavage formation in very low-grade metamorphic slates. *Tectonophysics* **78**, 291–306.
Wenk, H.-R. 1985. Measurement of pole figures. In: *Preferred Orientation in Deformed Metals and Rocks: An Introduction to Modern Texture Analysis* (edited by Wenk, H.-R.). Academic Press, Orlando, 11–47.
White, S. H. & Johnston, D. C. 1981. A microstructural and microchemical study of cleavage lamellae in a slate. *J. Struct. Geol.* **3**, 279–290.
White, S. H. & Knipe, R. J. 1978. Microstructure and cleavage development in selected slates. *Contr. Miner. Petrol.* **66**, 165–174.
White, S. H., Shaw, H. F. & Huggett, J. M. 1984. The use of backscattered electron imaging for the petrographic study of sandstones and shales. *J. sedim. Petrol.* **54**, 487–494.
Williams, P. F. 1972. Development of metamorphic layering and cleavage in low-grade metamorphic rocks at Bergagui, Australia. *Am. J. Sci.* **272**, 1–47.
Wood, D. S. 1974. Current views of the development of slaty cleavage. *Annu. Rev. Earth & Planet. Sci.* **2**, 369–401.
Wood, D. S. & Oertel, G. 1980. Deformation in the Cambrian slate belt of Wales. *J. Geol.* **88**, 309–326.
Wood, D. S., Oertel, G., Singh, J. & Bennet, H. F. 1976. Strain and anisotropy in rocks. *Phil. Trans. R. Soc. Lond.* **A283**, 27–42.
Woodcock, N. H. 1977. Specification of fabric shapes using an eigenvalue method. *Bull. geol. Soc. Am.* **88**, 1231–1236.
Woodcock, N. H. & Naylor, M. A. 1983. Randomness testing in three dimensional orientation data. *J. Struct. Geol.* **5**, 539–548.
Woodland, R. G. 1982. Gradational development of domainal slaty cleavage, its origin and relation to chlorite porphyroblasts in the Martinsburg Formation, eastern Pennsylvania. *Tectonophysics* **82**, 89–124.
Wright, T. O. & Platt, L. B. 1982. Pressure dissolution and cleavage in the Martinsburg slate. *Am. J. Sci.* **282**, 122–135.

* In Japanese with English abstract.
† In Japanese.

APPENDIX

Reliability of measurement techniques of X-ray texture goniometry

The combined reflection–transmission mode scan method was used in this study for measurement of phyllosilicate preferred orientation because of its advantages described in Siddans (1976, 1978). Sections parallel to cleavage were used as specimens for texture goniometry because of easy specimen preparation. However, Oertel (1978, 1983) and Oertel *et al.* (1989) argued that phyllosilicate preferred orientation should be measured only in transmission mode, because scanning in reflection mode would preferentially sample the specimen surface region where phyllosilicate grains are mechanically disturbed by grinding or polishing. The reliability of the measurement technique used in this study was therefore investigated.

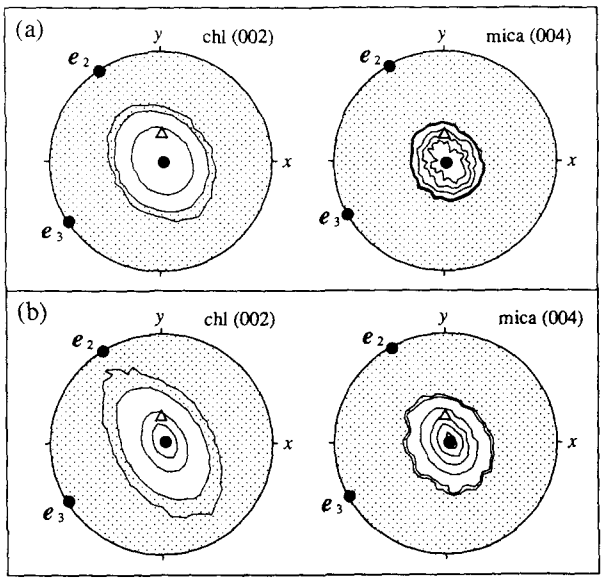

Fig. A1. Pole figures of chlorite (002) and illite/mica (004) basal planes obtained from the cleavage-parallel section (a) and the cleavage-normal section (b). Lower-hemisphere equal-area projections. Contours at 0.5, 1, 5, 10, 15 and 20 in multiples of a random distribution density. Areas with pole densities less than the random distribution density (<1) are stippled. Open triangle: pole of bedding; closed circles: eigenvectors of orientation tensor.

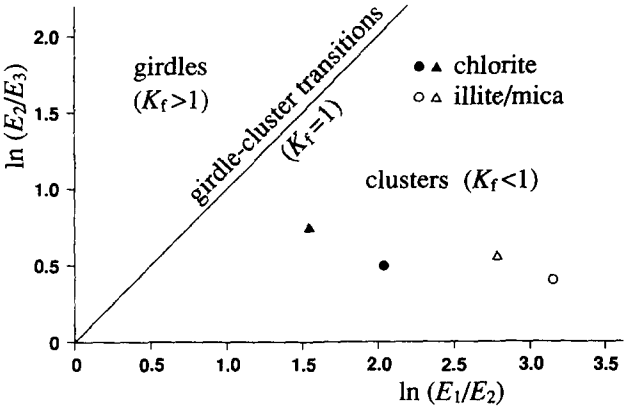

Fig. A2. Logarithmic eigenvalue ratio plot of orientation tensors calculated from pole figure data of chlorite and illite/mica. Circles: cleavage-parallel section; triangles: cleavage-normal section.

Two circular sections of known orientations, one cleavage-parallel and the other cleavage-normal, were prepared from a sample using the procedure described in the text. The cleavage-parallel section was scanned using the technique described in the text. The cleavage-normal section was scanned with both 5° tilt and azimuth intervals also in mixed reflection and transmission modes. In this case, reflection scan covers the central part of pole figure with polar angles of 0–30°, while transmission scan covers the peripheral part with polar angles of 30–90°. This covers most directions of phyllosilicate basal planes by the transmission scan. A complete measurement took 14 h for chlorite and 40 h for illite/mica. Pole figures obtained from the cleavage-normal section were then rotated so that they were projected on exactly the same plane as the cleavage-parallel section. Chlorite and illite/mica pole figures obtained from these two sections and their eigenvalue ratio plots are shown in Figs. A1 and A2.

Phyllosilicate basal plane fabrics of the cleavage-parallel section differ in both pattern and strength from those of the cleavage-normal section. Both chlorite and illite/mica fabrics obtained from the cleavage-parallel section are slightly closer to uniaxial clusters with

smaller K_f values and a greater fabric strength with higher $\bar{\epsilon}_f$ values than the corresponding fabrics obtained from the cleavage-normal section (Figs. A1 and A2). The irradiated volume fraction from the ground specimen surface in reflection mode must contribute to these discrepancies. This indicates that phyllosilicate grains on the specimen surface are aligned parallel to the surface due to grinding even after being vacuum-impregnated with epoxy. The cleavage-parallel section would be more easily affected by this grinding effect, because most phyllosilicates on the surface are already aligned subparallel to the surface so that they are easily smeared into parallelism with the ground surface. The phyllosilicates are mostly aligned subperpendicular to the surface of the cleavage-normal section so that they can hardly be rotated into parallelism with the surface. The combined reflection–transmission mode method may therefore be adequate for phyllosilicate preferred orientation measurement of cleavage-normal sections.

In spite of the discrepancies above, there is a good correlation in pattern and strength between the phyllosilicate basal plane fabrics obtained from the two sections. The eigenvectors determined from the former precisely coincide with the corresponding ones of the latter (Fig. A1). The fabrics of the cleavage-parallel section are not significantly different in pattern from those of the cleavage-normal section. Phyllosilicate preferred orientation measurement of cleavage-parallel sections using combined reflection–transmission mode method is therefore acceptable as far as relative variations in fabric pattern and strength are examined. But particular care must be taken in comparing the results with strain data, because the K_f values are underestimated.